CHAPTER - 7

SPIN RELAXATION OF $Gd_2O_3/NiFe_2O_4$ CORE-SHELL NANOPARTICLES

7.1 Introduction

In recent years, science and technology have considerably developed and have created various nanomaterials such as NPs [1, 2], nanotubes [3, 4], nanofilms [5, 6], graphene [7, 8] and nanoporous materials [9, 10]. Among them, the core-shell nanoparticles (CSNPs) with magnetic components have attracted much interest in recent years in both fundamental research [11, 12] and practical applications [13, 14]. The CSNPs having magnetic core and non-magnetic shell have also been investigated for biological applications [15]. However, magnetic properties of the inverse structure, such as, NPs with a non-magnetic core and a magnetic shell have rarely been studied. In most of the cases, the synthesis of the particles is complicated and expensive. Here, we report the synthesis and the properties of non-magnetic/magnetic CSNPs consisting of nonmagnetic core of gadolinium oxide (Gd_2O_3) which is encapsulated in magnetic shell of nickel ferrite ($NiFe_2O_4$). We employed polyol method as a cost effective and versatile synthesis method. These CSNPs can be used as contrast agent to improve the visualization of magnetic resonance imaging (MRI) which is a diagnostic technique widely employed due to its capability to distinguish between healthy and pathological tissues.

The use of contrast agent for MRI depends on the ability of the agent to shorten the relaxation times (T_1 and T_2) of water protons. Each distinct tissue type has unique relaxation rates ($1/T_1$ and $1/T_2$) and a proton density which affect tissue contrast and image interpretation [16]. Relaxation rates $1/T_1$ and $1/T_2$ measure the rate that molecular spins after being perturbed by the radio-frequency wave inside a magnet return back to their energy equilibrium states. T_1 is called spin-lattice

relaxation time that is the time needed for spins and their environment (dubbed "lattice") to reach energy equilibrium. T_2 is called spin-spin relaxation time and it is time for spins themselves to reach equilibrium after radio frequency wave perturbation. In the core/shell of $Gd_2O_3/NiFe_2O_4$, Gd_2O_3 can serve as positive contrast agent to reduce T_1 relaxation time resulting in a brighter signal, while magnetic $NiFe_2O_4$ can act as negative contrast agent to reduce T_2 relaxation time resulting in a darker signal [17, 18]. In the present work, we demonstrate the combined effect of two different relaxation characteristics in $Gd_2O_3/NiFe_2O_4$ CSNPs employing electron paramagnetic resonance (EPR) spectroscopy which is a powerful tool in the investigation of magnetic properties and spin dynamics in condensed matter.

7.2 Experimental Procedure

$Gd(NO_3)_3.6H_2O$ (Alfa Aesar), $Ni(NO_3)_2.6H_2O$ (Alfa Aesar) and $FeCl_3$ (Merck) of reagent grades were used as the starting materials. Polyethylene glycol 400 (PEG) was used as a solvent and doubly distilled water and ethanol were employed for the washing. For the synthesis of $NiFe_2O_4$ and Gd_2O_3 NPs, 4 mM of $Ni(NO_3)_2.6H_2O$ along with 8 mM of $FeCl_3$ and 12 mM of $Gd(NO_3)_3.6H_2O$ were dissolved separately in 30 ml of polyethylene glycol (PEG) under stirring in a round bottomed flask at 100 ^oC. The clear transparent salt solutions obtained were subsequently heated to 180 ^oC for 90 min. The resulting reddish brown solution of $NiFe_2O_4$ and brown suspension of Gd_2O_3 were cooled to room temperature, diluted with ethanol and the NPs were separated from the solutions by centrifugation at 10,000 rpm. To remove unreacted precursor and PEG, the sediment materials were dispersed in ethanol and centrifuged at three times. The materials obtained after centrifugation were calcined at 600 ^oC for 2 h in air. To get the NPs of $Gd_2O_3/NiFe_2O_4$ core/shell, $NiFe_2O_4$ shell was grown on the core Gd_2O_3 employing a two step process. Firstly, the as-prepared Gd_2O_3 core

NPs was dispersed in 25 ml of PEG under sonication for 10 minutes and then a solution of PEG (15 ml) containing 4 mM of $Ni(NO_3)_3.6H_2O$ and 8 mM of $FeCl_3$ was injected into the dispersed nanocore system. After mixing the above solution (using a magnetic stirrer for 15 min), the mixed system was heated at 180 ^oC for 2 h and cooled down to room temperature, washed, centrifuged and after that calcined at 600 ^oC for 2 h in air to get $Gd_2O_3/NiFe_2O_4$ CSNPs. The phase purity and crystal structure of the synthesised samples were analysed by powder X-ray diffractometer (Rigaku Miniflex-II) operating at 30 kV/15mA using Cu-K_α radiation (wavelength = 1.5416 Å) in the scanning range of $20^o \leq 2\theta \leq 70^o$ with a scanning step of 0.04^o at room temperature. The micro-structural investigation of the NPs was done using transmission electron microscope (TEM) (Technai G2 TF20ST) operating at 200 kV. Variable temperature EPR spectra were recorded from 300 K to 110 K during cooling by a Bruker EMX plus spectrometer operating at X-band (frequency = 9.43 GHz) with 100 kHz magnetic field modulation. Magnetic characterisation of the NPs was carried out using an ADE EV9 model vibrating sample magnetometer (VSM) by applying a maximum field of 20 kOe.

7.3 Results and Discussion

7.3.1 Structural and Micrographical Studies

Figure 7.1a shows the X-ray diffraction pattern of the Gd_2O_3 NPs where the major peaks are obtained at 2θ = 28.50º, 33.06º, 35.26º, 42.69º, 47.44º, 52.21º and 56.34º corresponding to (222), (400), (411), (134), (440), (611) and (622) crystal planes. The nature and position of the above diffraction peaks are the characteristic of cubic gadolinium oxide phase as per JCPDS card file number: 43-1014. Typical XRD pattern of $NiFe_2O_4$ NPs (Figure 7.1b) shows existence of strong and sharp diffraction peaks at 2θ values 30.12º, 35.56º and 63.08º and its crystal planes are (220), (311) and

(440) respectively and these peaks are matched with JCPDS card number: 86-2267. Gd_2O_3 and $NiFe_2O_4$ diffraction patterns are observed in the $Gd_2O_3/NiFe_2O_4$ core/shell system (Figure7.1c) but its diffraction angles are slightly shifted from their bare one.

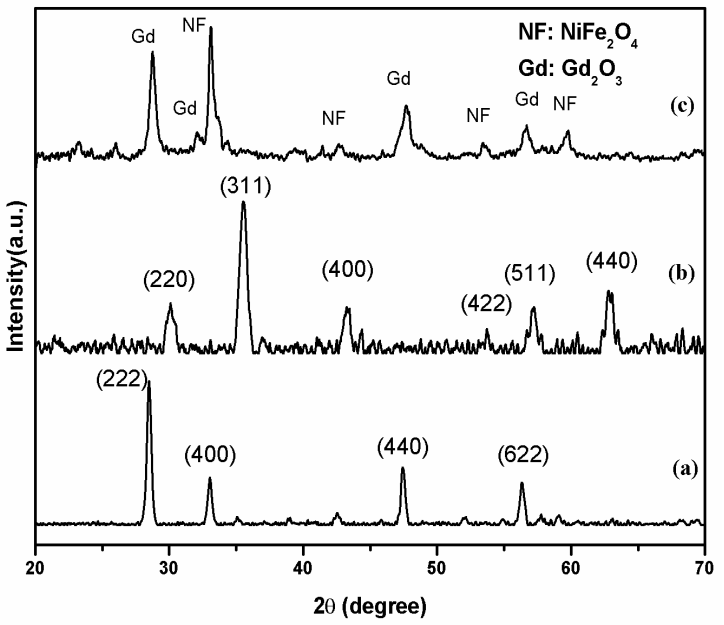

Figure 7.1 X-ray diffraction patterns of (a) Gd_2O_3, (b) $NiFe_2O_4$ and (c) $Gd_2O_3/NiFe_2O_4$ NPs

The evidence of peak shifting has been reported by Cao and Banin in a different core/shell system where the diffraction peaks shift to higher 2θ angles because of the strain from epitaxial growth of an InP shell on an InAs core [19]. In the present system, the shift in the diffraction peaks at lower angle may be due to the very small thickness of the shell material on the core NPs. Thus, the development of the strain due to the epitaxial growth of shell material on the core is strongly affected and is observed in the diffraction pattern of these CSNPs.

The ordinary TEM micrograph is shown in Figure 7.2a which clearly displays the core-shell morphology of well dispersed $Gd_2O_3/NiFe_2O_4$ NPs. The average particle diameter increases from 6 nm for the spherical Gd_2O_3 core particles to 12 nm for the slightly elongated $Gd_2O_3/NiFe_2O_4$ CSNPs. The presence of lattice fringes in

the high-resolution TEM (HRTEM) micrograph of Gd_2O_3 core as shown in Figure 7.2b indicates that these NPs possess high crystalline.

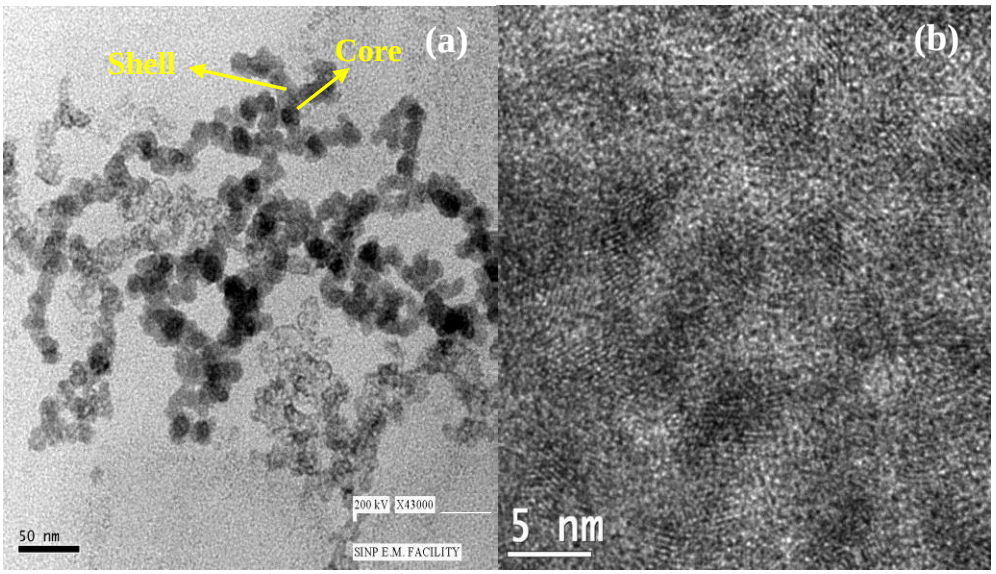

Figure 7.2 (a) TEM micrograph obtained for $Gd_2O_3/NiFe_2O_4$ CSNPs (b) HRTEM micrograph obtained for Gd_2O_3 core

7.3.2 Magnetic Studies

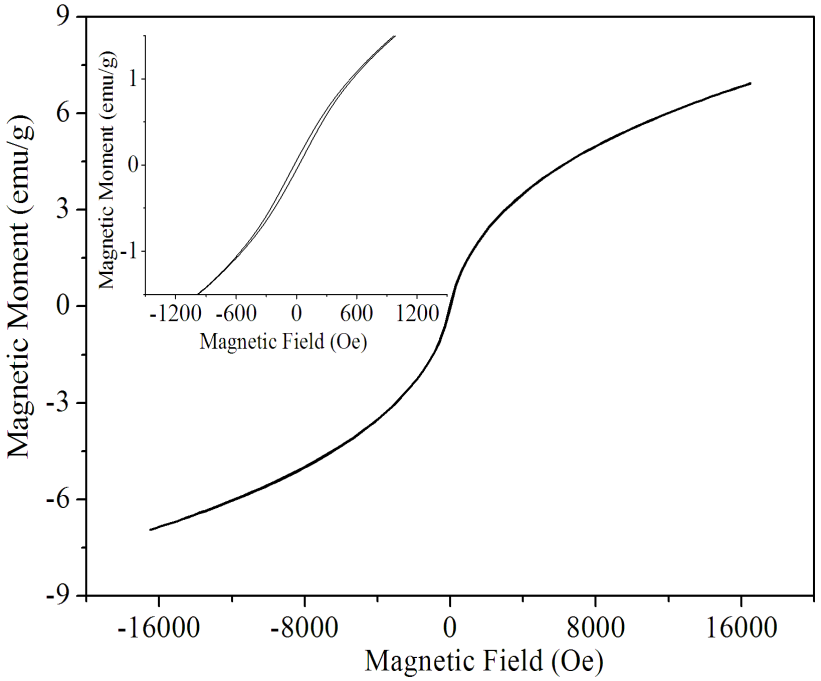

Figure 7.3 Room temperature hysteresis curve obtained for $Gd_2O_3/NiFe_2O_4$ CSNPs The inset Figure shows the hysteresis plot for the lower values of the magnetic field

Room temperature hysteresis curve of $Gd_2O_3/NiFe_2O_4$ CSNPs is shown in Figure 7.3. It is observed that the magnetization does not saturate for the material even at highest field of 2 Tesla. Thus, the saturation magnetization (M_s) is evaluated using the following equation [20]:

$$M=M_s (1-a/H) \text{ ……. } (7.1)$$

Where, „M_s" is the saturation magnetization and „a" is a fitting parameter. In the high field region, the plot between M and 1/H gives a straight line whose intersection with 1/H = 0 axis will give the value of M_s. The values of saturation magnetization (M_s) and coercivity (H_c) are found to be 6.96 emu/g and 25 Oe respectively. The inset of Figure 7.3 shows more clearly the appearances of the hysteresis loop in the sample when the data are plotted for the lower values of the magnetic field. It is to be mentioned that NPs (~ 10 nm) of pure $NiFe_2O_4$ show superparamagnetic behaviour at room temperature [21]. The same is not observed for the present system because Gd_2O_3 has modulated the magnetic properties of $NiFe_2O_4$.

7.3.3 Electron Paramagnetic Resonance Studies

Typical first derivative EPR spectra of the $Gd_2O_3/NiFe_2O_4$ CSNPs in the temperature range of 110 K - 300 K are shown in Figure 7.4. The EPR spectra obtained for the CSNPs show the single resonance from 300 K to 150 K. The spectrum at 110 K contains an additional small signal in the higher magnetic field region corresponding to the resonance at around 4500 Gauss. It may be due to the anisotropy character arising on the surface of NPs at low temperature [22]. The line width of the EPR signal is found to decrease with the increase of temperature. At low temperature, the line width is large due to the scattering in the direction of anisotropic field of particles. As the temperature increases, a tendency to make the magnetic moment isotropic is developed causing a decrease in the line widths [23]. Figure 7.5a

shows the variation in the peak-to-peak linewidth (ΔH_{pp}) with temperature. The value of ΔH_{pp} continuously decreases with increasing temperature. The direction of magnetization in NPs fluctuates at a rate faster than the Larmor frequency, resulting in a narrow resonance line due to an average effect of this fluctuation on the magneto crystalline anisotropy. Dixit *et al*. [24] have found that the bare $NiFe_2O_4$, Gd^{3+} and Ce^{3+} doped $NiFe_2O_4$ have the ΔH_{pp} values of 2100, 1600 and 1400 Gauss respectively at room temperature. The $NiFe_2O_4$ encapsulated Gd_2O_3 CSNPs exhibit smaller (600 Gauss) than the above rare earth doped $NiFe_2O_4$ system, which is an important factor for the application of this material in the microwave region [25]. The lowest loss observed in this CSNP is associated with the more number of rare earth atoms present in the core.

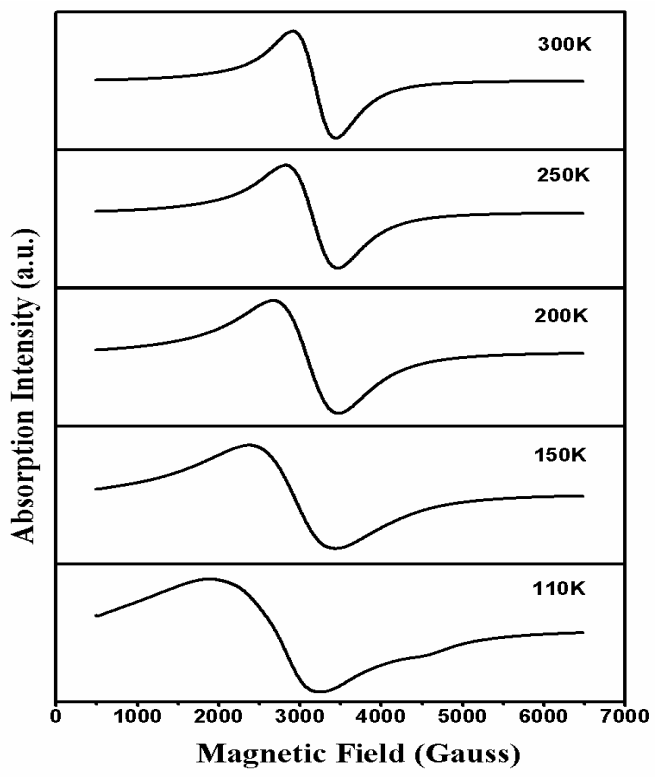

Figure 7.4 EPR spectra obtained for $Gd_2O_3/NiFe_2O_4$ CSNPs at low temperatures

The energy difference between two adjacent degenerate spin energy levels „ΔE‟ has the same behaviour as of the line width. The reduction of line width may cause a reduction in ΔE value. The value of ΔE is given by the relation $\Delta E = h\nu = g\mu_B H_0$ [26]. Thus, the „g‟ value is defined as the constant of proportionality between the frequency and the field at which resonance occurs, and is proportional to the magnetic moment of the molecule being studied. On the other hand, the „g‟ value of the EPR signal is a function of the molecular motion, the paramagnetic properties and the symmetry of ions [27]. It has been observed from Figure 7.5b that the g value increases with decreasing temperature. Both peak-to-peak linewidth (ΔH_{pp}) and g-value increase with decreasing temperature which depend upon two main factors namely magnetic dipole interactions among the particles and exchange interaction between the ions. Strong dipole interaction gives a large ΔH_{pp} and strong super-exchange interaction produces a small ΔH_{pp} [28].

7.3.3.1 Variation of Spin-Spin Relaxation Time (T_2) with Temperature

It is well known that there are two relaxation processes in EPR system *viz*. spin-lattice and spin-spin interactions. If the line width of the EPR is determined by spin-spin relaxation, line width increases with decreasing temperature. In the present system, linewidth increases rapidly with decreasing temperature, therefore it may not be associated with the spin-lattice relaxation that plays a dominant role, but the other mechanism, namely, the spin-spin relaxation should be operative. If involved spins are like the magnetic exchange interaction it causes a broadening of resonance lines as the temperature increases. On the contrary, if the magnetic exchange takes place between „unlike spins‟ a narrowing of resonance lines will be caused when the temperature is increased. The observed narrowing of the EPR peaks with the increasing temperature in the present case may be attributed to the exchange

interaction between unlike spins. The spin relaxation process is characterised by a time constant, which is a function of static magnetic field and depends on the rate at which microwave energy can be absorbed and dissipated. The spin-spin relaxation process is the energy difference transferred to the neighboring electrons and the relaxation time (T_2) can be determined from the peak-to-peak line-width according to the formula as follows [22]:

$$1/T_2 = g\,\mu_B\,\Delta H/\hbar \quad \ldots\ldots\ldots \quad (7.2)$$

where ΔH is the full width at half maxima of the absorption peak, μ_B is Bohr magnetron.

Figure 7.5d shows the variation of T_2 with temperature of $Gd_2O_3/NiFe_2O_4$ CSNPs. The increase in temperature should increase the motion of electrons causing stronger superexchange interactions among the cations through oxygen ions, and a decrease in ΔH_{pp} and g_{eff} value and hence the T_2 value increases with increasing temperature. In core-shell magnetic NPs system, the interfacial exchange coupling between core and shell region increases with decreasing temperature resulting in the decrease in the time of relaxation and thus broadened the EPR spectrum line as observed. Sundaresan *et al*. [29] have reported that the NPs of metal oxide show room temperature ferromagnetism due to the exchange interaction between unpaired electron spins arising from oxygen vacancies at the surfaces of the NPs. Ong and Wei [30] have reported that the exchange coupling between core and shell regions is strong below the room temperature. In this condition, magnetic dipole interaction between the particles may be dominant. $NiFe_2O_4$ has the intrinsic moment 2.2 μ_B, so the magnetic dipolar interactions among these particles are strong thus increasing the value of ΔH_{pp} and g_{eff} with decreasing temperature.

The Gd_2O_3 and magnetic $NiFe_2O_4$ NPs are the T_1 and T_2 relaxation characteristics respectively [17, 18]. In the present studies, combined system of these materials in the form of core-shell nanostructure showed the T_2 relaxation characteristics. It reveals that the shell material properties are dominating over the core material properties in this $Gd_2O_3/NiFe_2O_4$ core-shell nanosystem and also the core material enhance the shell material properties.

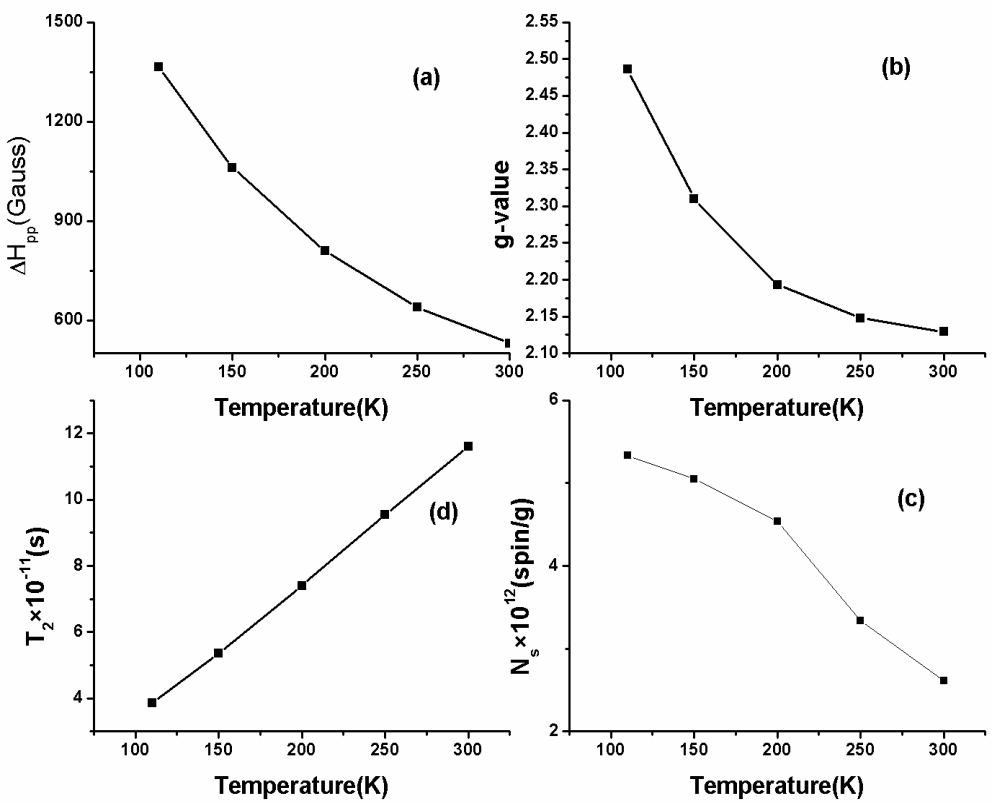

Figure 7.5 Variation of (a) peak to peak line width (ΔH_{pp}) with temperature, (b) g-factor with temperature, (c) spin concentration (N_s) with temperature and (d) relaxation time (T_2) with temperature for $Gd_2O_3/NiFe_2O_4$ CSNPs

The EPR spin number is the area under an EPR absorption curve, which is proportional to the number of unpaired spins in the sample. The EPR spin number is calculated as the product of ΔH_{pp}^{2} h, where h is peak-to-peak height [31]. It is seen from Figure 7.5c that the spin number increases with decreasing temperature. In this CSNPs system, it is observed that there is an increase in the exchange coupling between core and shell region during lowering of the temperature which causes an increase in the N_s value due to the uncompensated magnetic moment arising at the interfacial region between the core and shell.

7.4 Conclusions

Well-crystalline $Gd_2O_3/NiFe_2O_4$ (core/shell) NPs have been successfully prepared by polyol process. The phase formation is confirmed by X-ray diffraction pattern. The particle size of the CSNPs is found to be ~ 12 nm. The temperature dependent EPR parameters ΔH_{pp}, g_{eff}, N_s and T_2 are studied in the temperature range from 110 K to 300 K. The values of ΔH_{pp}, g-factor and N_s are increased whereas T_2 value is decreased with the decrease of temperature. These results are due to the enhancement of dipolar interactions and interfacial exchange coupling between the core and shell regions below the room temperature. The $Gd_2O_3/NiFe_2O_4$ CSNPs show the lowest loss at 300 K and it is associated with the more number of rare earth atoms present in these CSNPs. VSM result shows that the saturation magnetization of these CSNPs is 6.96 emu/g. In this core-shell nanosystem, the interfacial exchange coupling between core and shell region increases with decreasing temperature resulting decrease in the T_2 relaxation time and thus broadening the EPR spectrum line as observed.

References

1. C. Li, C. Ma, F. Wang, Z. Xi, Z. Wang, Y. Deng and N. He, J. Nanosci. Nanotechnol. 12 (2012) 2964.
2. S. Krol, R. Macrez, F. Docagne, G. Defer, S. Laurent, M. Rahman, M. J. Hajipour, P. G. Kehoe and M. Mahmoudi, Chem. Rev. 113 (2013) 1877.
3. T. Fujigaya and N. Nakashima, J. Nanosci. Nanotechnol. 12 (2012) 1717.
4. V. Castranova, P. A. Schulte and R. D. Zumwalde, Acc. Chem. Res. 46 (2013) 642.
5. K. Ariga, Q. Ji, J. P. Hill, Y. Bando and M. Aono, NPG Asia Mater. 4 (2012) e17.
6. K. Ariga, T. Mori and J. P. Hill, Adv. Mater. 24 (2012) 158.
7. L. Zhang, Y. Xing, N. He, Y. Zhang, Z. Lu, J. Zhang and Z. Zhang, J. Nanosci. Nanotechnol. 12 (2012) 2924.
8. J. N. Coleman, Acc. Chem. Res. 46 (2013) 14.
9. K. Ariga, A. Vinu, Y. Yamauchi, Q. Ji and J. P. Hill, Bull. Chem. Soc. Jpn. 85 (2012)1.
10 L. Chu and X. Zhang, J. Nanosci. Nanotechnol. 12 (2012) 300.
11. H. Zeng, S. Sun, J. Li, Z. L. Wang and J. P. Liu, Appl. Phys. Lett. 85 (2004) 792.
12. R. G. Chaudhuri and S. Paria, Chem. Revs. 112 (2012) 2373.
13. V. S. Maceira and M. A. Correa-Duarte, Adv. Mater. 19 (2007) 4131.
14. S. Wei, Q. Wang, J. Zhu, L. Sun, H. Lin and Z. Guo, Nanoscale, 3 (2011) 4474.
15. D. Dosev, M. Nichkova, R. K. Dumas, S. J. Gee, B. D. Hammock, K. Liu and I. M. Kennedy, Nanotechnology, 18 (2007) 055102.
16. N. G. C. Thiang, COSMOS, 8 (2012) 103.
17. H. Gustafsson, M. Ahren, F. Soderlind, J. M. C. Gallego, P. O. Kall, P. Nordblad, P. O. Westlund, K. Uvdal and M. Engstrom, J. Phys. Chem. C, 115 (2011) 5469.
18. D. Zhu, F. Liu, L. Ma, D. Liu and Z. Wang, Int. J. Mol. Sci. 14 (2013) 10591.
19. Y. W. Cao and U. Banin, J. Amer. Chem. Soc. 122 (2000) 9692.
20. G. Dixit, J. P. Singh, R. C. Srivastava, H. M. Agarwal, R. J. Choudhary and A. Gupta, Indian J. Pure & Appl. Phys. 48 (2010) 287.
21. O. V. Yelenich, S. O. Solopan, T. V. Kolodiazhnyi, V. V. Dzyublyuk, A. I.

Tovstolytkin and A. G. Belous, Sol. State Sci. 20 (2013) 115.

22. J. P. Singh, R. C. Srivastava and H. M. Agarwal, Int. J. Nanosci. 8 (2009) 523.
23. R. Massart, D. Zins, F. Gendron, M. Rivoire, R. V. Mehta, R. V. Upadhyay, P. S. Goyal and V. K. Aswal, J. Magn. Magn. Mater. 201 (1999) 73.
24. G. Dixit, J. P. Singh, R. C. Srivastava and H. M. Agarwal, J. Magn. Magn. Mater. 324 (2012) 479.
25. S. C. Byeon, K. S. Hong and I. T. Kim, J. Appl. Phys. 83 (1998) 6873.
26. J. F. Raber, Experimental Methods in Polymer Chemistry-Physical Principal and Applications, Wiley, Newyork (1980).
27. J. W. Stucki and W. L. Banwart, Advanced Chemical Methods for soil and Clay Mineral Research, Reidel, Dordrecht (1980).
28. L. Li, G. Li, R. L. Smith and H. Inomata, Chem. Mater. 22 (2000) 3705.
29. A. Sundaresan, R. Bhargavi, N. Rangarajan, U. Siddesh and C. N. R. Rao, Phys. Rev. B, 74 (2006) 161306(R).
30. Q. K. Ong and A. Wei, Phys. Rev. B, 80 (2009) 134418.
31. K. H. Wu, Y. C. Chang, H. B. Chen, C. C. Yang and O. N. Horng, J. Magn. Magn. Mater. 278 (2004) 156.